



Supporting Information

Chiral Phosphoric Acid Catalyzed Asymmetric Hydrolysis of Biaryl Oxazepines for the Synthesis of Axially Chiral Biaryl Amino Phenol Derivatives

L. Wei, J. Li, Y. Zhao, Q. Zhou, Z. Wei, Y. Chen, X. Zhang, X. Yang**

racemization (k_{rac}), and half-life for racemization ($t_{1/2rac}$) were calculated based on the following equations,

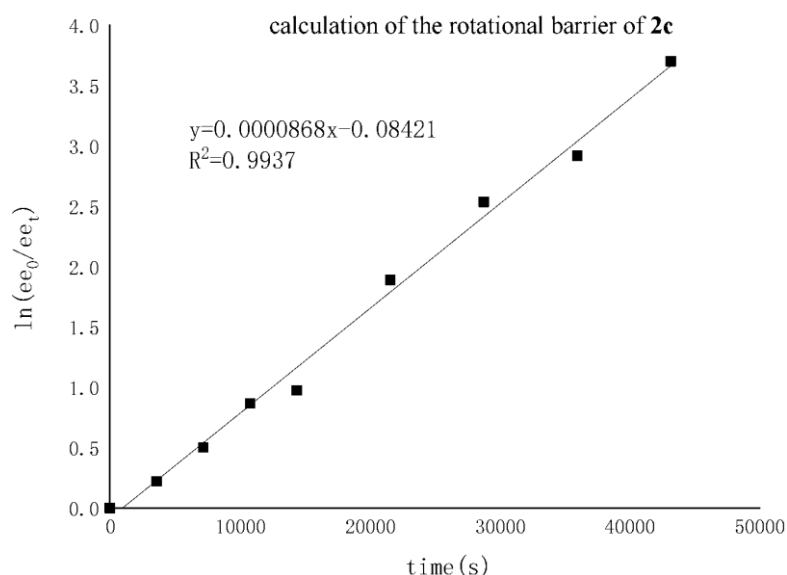
$$t_{1/2rac} = \ln 2 / k_{rac}$$

$$\Delta G^\ddagger = -RT \ln(k_{ent} h / k_B T)$$

where the transmission coefficient κ is set as 1, Boltzmann constant $k_B = 1.3806503 \times 10^{-23}$ J/K, Planck constant $h = 6.62606876 \times 10^{-34}$ J·s, idea gas constant $R = 8.314472$ J/(mol·K).^[5]

Table. Change of enantiomer ratio with time for **2c** (120 °C in toluene)

t/s	ee(%)	ln (ee ₀ /ee _t)
0	95.180	0
3600(1 h)	76.266	0.22154
7200(2 h)	57.542	0.50325
10800(3 h)	40.020	0.86639
14400(4 h)	35.906	0.97486
21600(6 h)	14.370	1.89063
28800(8 h)	7.532	2.53661
36000(10 h)	5.138	2.91911
43200(12 h)	2.348	3.70221



$$\ln(ee_0/ee_t) = 2k_{ent}t + C$$

$$k_{ent} = 1/2 \text{ slope} = 0.0000434 \text{ s}^{-1}$$

$$k_{rac} = 2k_{ent} = 0.0000868 \text{ s}^{-1}$$

$$t_{1/2rac} = \ln 2 / k_{rac} = 7986 \text{ s} = 2.22 \text{ h}$$

$$\Delta G^\ddagger = -RT \ln(k_{ent} h / k_B T) = 31.1 \text{ kcal/mol}$$

DFT calculations

Conformational sampling

Conformational sampling of the phosphoric acid catalyst was carried out at GFN2-xTB^[6-8] level of theory using the CREST program version 2.12 by Grimme and co-workers.^[9,10] The conformers and rotamers ensemble was generated using the iterative

metadynamics based on genetic z-matrix crossing algorithm (iMTD-GC). Conformers were further optimized at GFN2-xTB level with very tight (*-opt vtight*) optimization. Due to the large size of the phosphoric acid catalyst, the lowest energy conformer was chosen and further optimized at density functional theory (DFT) level and used for the mechanistic studies.

Density functional theory (DFT) calculations

DFT calculations were carried out using the *Gaussian 16* rev. B.01 program.^[11] The global hybrid functional M06-2X^[12] with Karlsruhe basis set of double- ζ valence def2-SVP^[13,14] for all atoms were employed for all gas-phase optimizations. Single point (SP) corrections were performed using M06-2X functional and def2-TZVP^[13] basis set for all atoms. The implicit SMD continuum solvation model^[15] was used to account for the solvent effect of cyclohexane solvent that was used in the experimental reactions. Gibbs energies were evaluated at the room temperature (reaction condition), using the entropic quasi-harmonic treatment scheme of Grimme,^[16] at a cut off frequency of 100 cm⁻¹. The free energies were further corrected using standard concentration of 1 mol/L, which was used in solvation calculations. Data analysis was carried out using the GoodVibes code version 3.1.1.^[16] Gibbs energies evaluated at SMD(cyclohexane)-M06-2X/def2-TZVP//M06-2X/def2-SVP level of theory are given in kcal mol⁻¹ and used for discussion throughout.

Non-covalent interactions (NCIs) were analyzed using NCIPLOT^[17] calculations. The *.wfn* files for NCIPLOT were generated at M06-2X/def2-SVP level of theory. NCI indices calculated with NCIPLOT were visualized at a gradient isosurface value of $s = 0.5$ au. These are colored according to the sign of the second eigenvalue (λ_2) of the Laplacian of the density ($\nabla^2\rho$) over the range of -0.1 (blue = attractive) to $+0.1$ (red = repulsive). Molecular orbitals are visualized using an isosurface value of 0.05 au throughout. All molecular structures and molecular orbitals were visualized using *PyMOL* software.^[18]

Computational rotational barriers studies

The rotational barriers for the enantiomerization of the substrate **1a** and the addition product **INT3** (Scheme S1) were studied computationally. First, a dihedral angle scan

along the axial C–C carbon bond was performed at M06-2X/def2-SVP in gas phase. The relaxed PES energy profile is shown in Figure S3. This gives an estimate of the rotational barrier of 20.0 kcal mol⁻¹. Using the structure with highest energy on this PES (i.e., structure 4 in Figure S3) as the initial guess structure for TS search, we successfully located the *true* TS for the enantiomerization via rotation along the axial C–C bond. After single point energy correction at higher basis set and with solvent effect at SMD(cyclohexane)-M06-2X/def2-TZVP, substrate **1a** was found to have a rotational barrier/enantiomerization barrier of $\Delta G^\ddagger = 17.4$ kcal mol⁻¹.

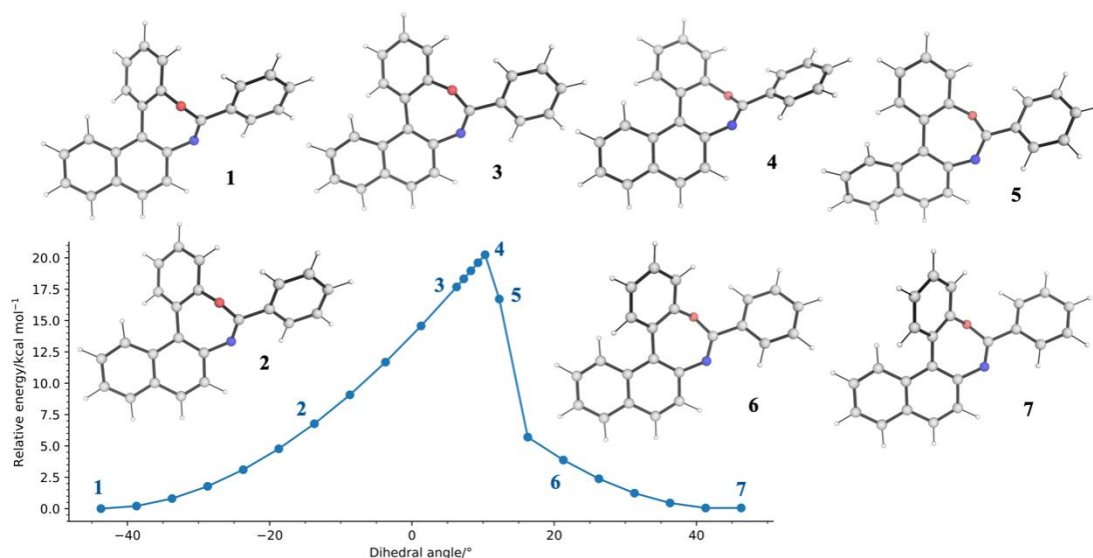


Figure S3. Relaxed potential energy surface (PES) scan for the dihedral angle along the C–C axial bond of substrate **1a**, computed at M06-2X/def2-SVP level of theory.

For intermediate **INT3**, we similarly studied the rotational barrier by first performing a dihedral angle scan along the axial C–C bond. The relaxed PES scan for **INT3** is shown in Figure S4. The highest energy structure on the scan PES was used as initial guess structure to locate the true TS for enantiomerization, which has a solvent corrected rotational barrier/enantiomerization barrier of $\Delta G^\ddagger = 24.2$ kcal mol⁻¹ (**TS_rot2**, Figure S5).

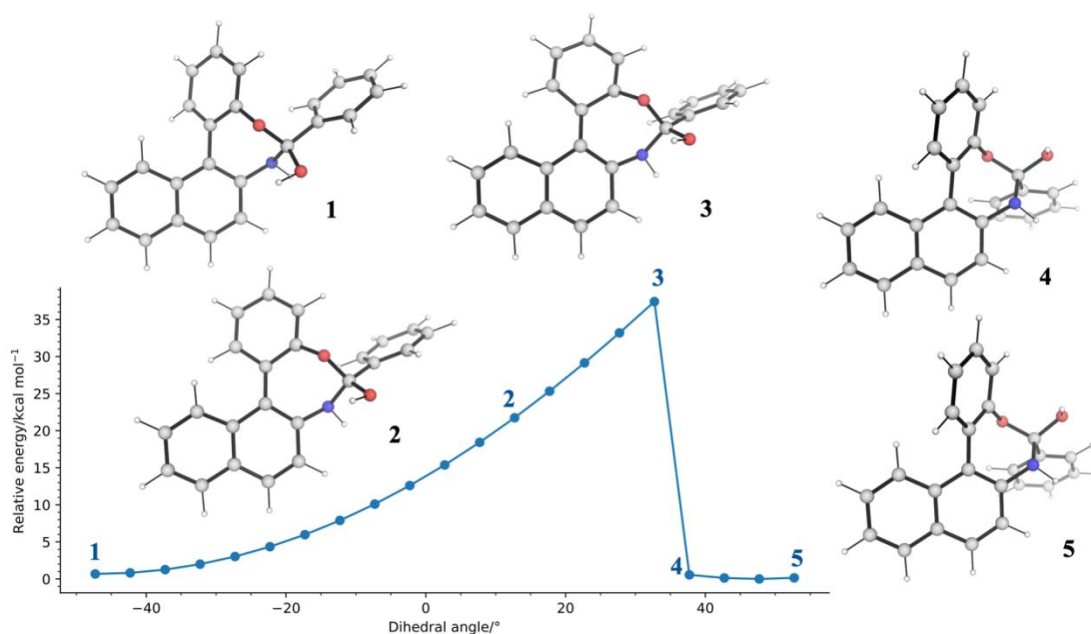
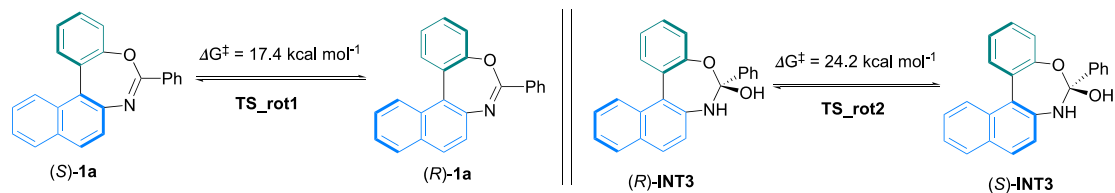


Figure S4. Relaxed potential energy surface (PES) scan for the dihedral angle along the C–C axial bond of intermediate **INT3**, computed at M06-2X/def2-SVP level of theory.

Figure S5 shows the DFT optimized structures of the transition states of the enantiomerization of these structures. The TSs for the enantiomerization for each of these structures have been successfully located and verified by intrinsic reaction coordinate (IRC)^[19,20] analyses (see attached IRC movies).



Scheme S1. Computed rotational barriers for the enantiomerization of substrate **1a** and intermediate **INT3**.

TS_rot1	TS_rot2
$\Delta G^\ddagger = 17.4 \text{ kcal mol}^{-1}$	$\Delta G^\ddagger = 24.2 \text{ kcal mol}^{-1}$

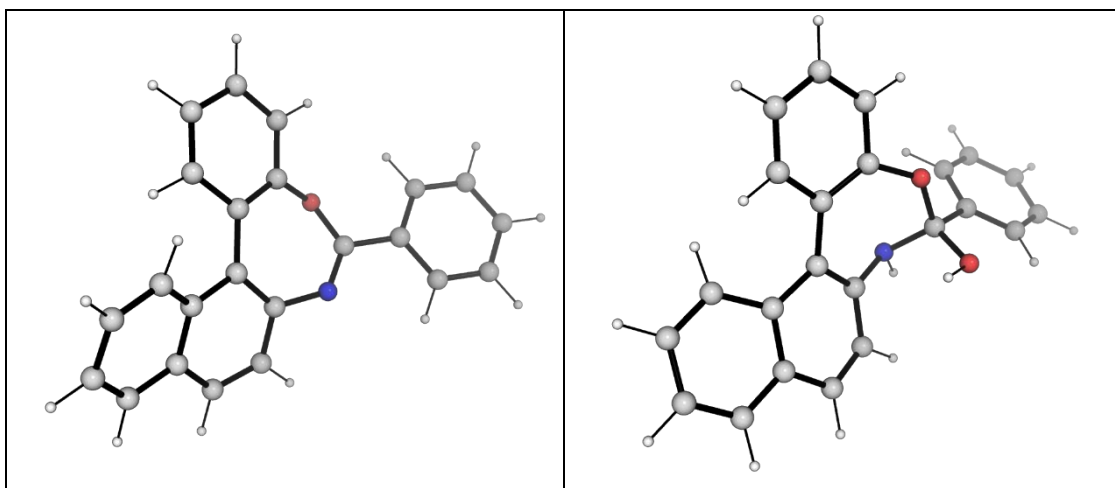


Figure S5. DFT-optimized transition state structures for the enantiomerization of substrate **1a** (**TS_rot1**) and intermediate **INT3** (**TS_rot2**). Computed rotational barriers are taken relative to each structure as reference zero. Rotational barriers are calculated at SMD(cyclohexane)-M06-2X/def2-TZVP//M06-2X/def2-SVP level of theory at room temperature and are given in kcal mol⁻¹.

The computed enantiomerization barrier for substrate **1a** at 17.4 kcal mol⁻¹ translates to a half-life of about 1 second at room temperature using simple transition state theory for estimation. Thus, substrate **1a** is expected to enantiomerize rapidly at the reaction condition and no enantiomeric excess (ee) can be observed at the reaction condition. On the other hand, the enantiomerization barrier of 24.2 kcal mol⁻¹ for **INT3** gives a half-life of about 17.5 hours, allowing (*R*)-**INT3** to react away via (*R*)-**TS2** (much lower barrier) more rapidly than it has time to enantiomerize to (*S*)-**INT3** via **TS_rot2** (Figure 3, main text).

We additionally studied the rotational barrier for substrate **1ai**, a relaxed PES dihedral angle scan along the C–C axial axis estimates a rotational barrier of ~60 kcal mol⁻¹ for substrate **1ai** (Figure S6). However, using the highest energy as a guess for TS location, no TS could be successfully located. This is expected and is consistent with previous study of such substrates that the presence of ortho-substituents on the biaryls provide steric hinderance to prevent the ease of enantiomerization via rotation along the C–C axial axis^[21] (the methyl group here provides even more steric hinderance than the hydroxyl group in the earlier study). We further estimated the rotational barrier by using the highest energy structure (structure 3 in Figure S6) directly (without further optimization) and running frequency calculations in gas-phase at M06-2X/def2-SVP

followed by solvent correction at SMD(cyclohexane)-M06-2X/def2-TZVP. This gives an estimated barrier of 62.5 kcal mol⁻¹. Therefore, substrate **1ai** is not expected to racemize under reaction conditions at room temperature (or other synthetically useful temperature, e.g., half-life of 115 days at 400 °C).

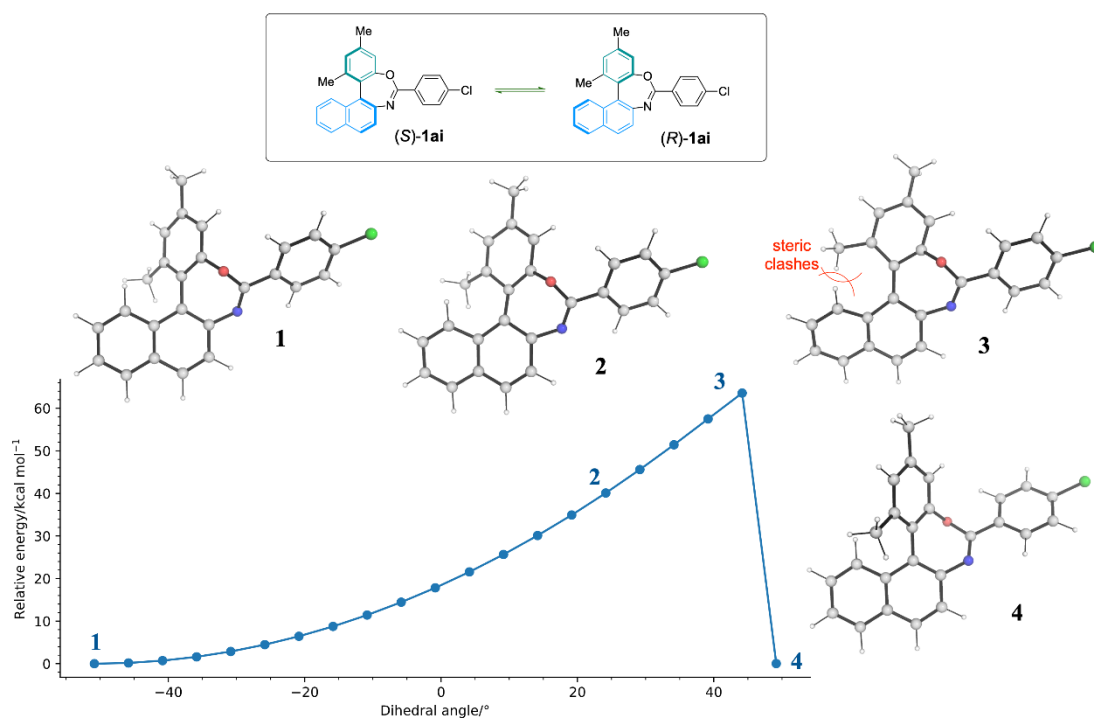


Figure S6. Relaxed potential energy surface (PES) scan for the dihedral angle along the C–C axial bond of substrate **1ai**, computed at M06-2X/def2-SVP level of theory.

Similarly, we studied the rotational barriers for the amide product arising from the reaction of substrate **1a**. The relaxed PES scan (Figure S7) suggests that the barriers for enantiomerization are > 30 kcal mol⁻¹, indicating that the product will be enantiostable at room temperature. The direct location of the TS for enantiomerization using the highest energy structures (structures 3 and 6, Figure S7) as initial guesses was unsuccessful; direct frequency calculations using these structures with solvent correction at SMD(cyclohexane)-M06-2X/def2-TZVP estimated the barriers to be 41.8 kcal mol⁻¹ and 34.7 kcal mol⁻¹, respectively, suggesting that the product is enantiostable at room temperature (and may be stable up to 150 °C with a half-life of ~18 hours).

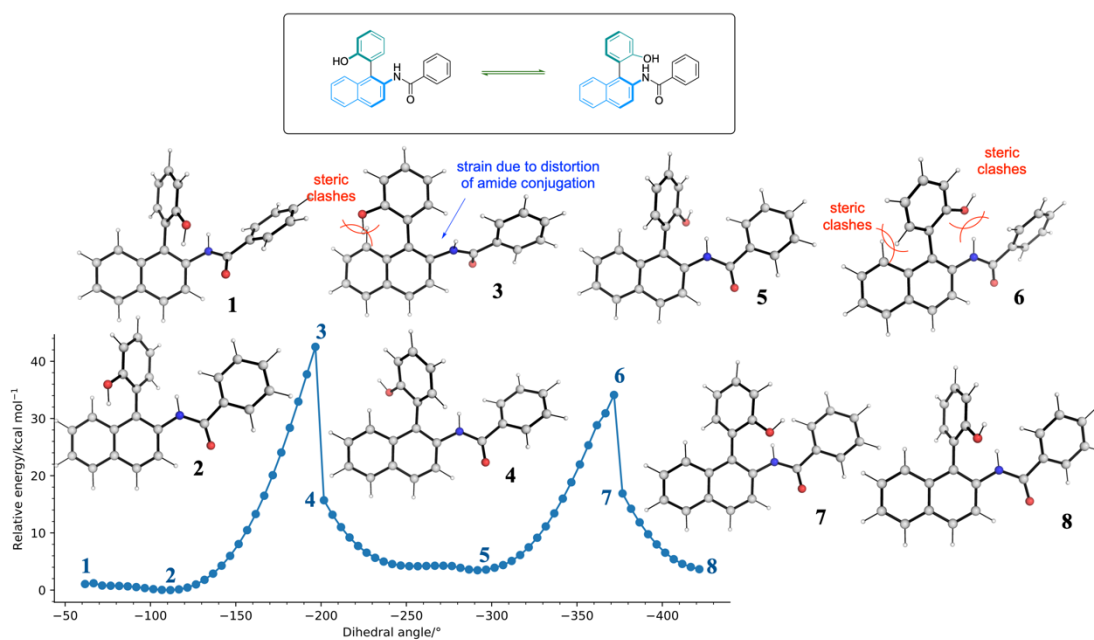
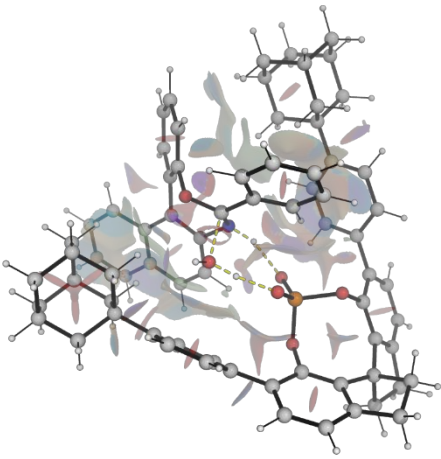
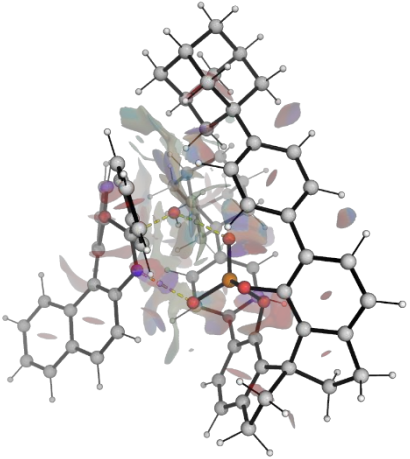

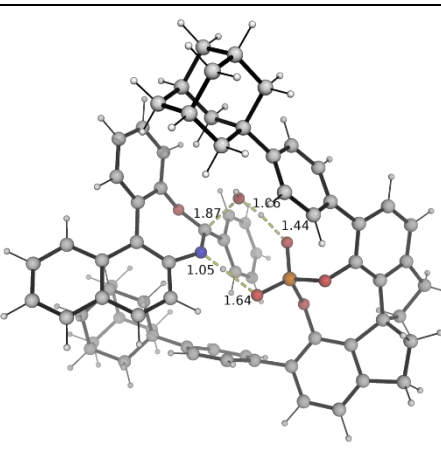
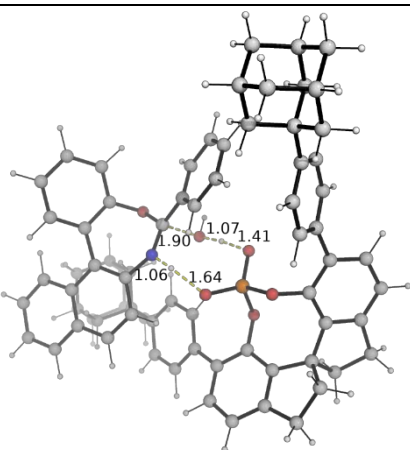
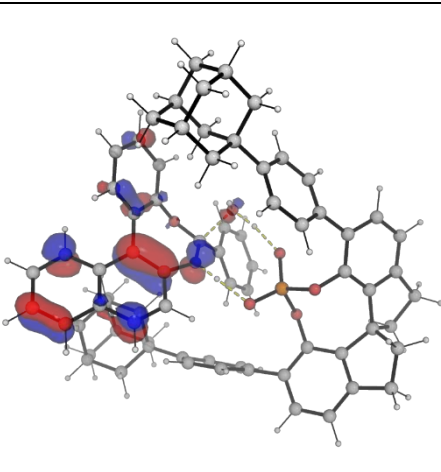
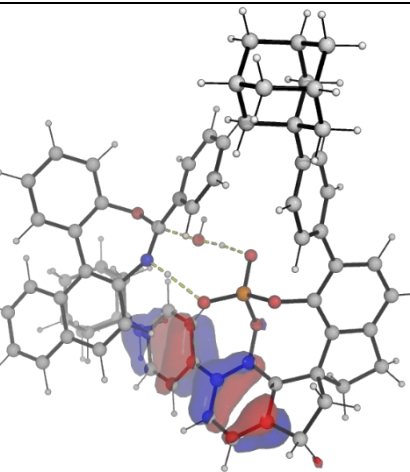


Figure S7. Relaxed potential energy surface (PES) scan for the dihedral angle along the C–C axial bond of the amide product of **2a**, computed at M06-2X/def2-SVP level of theory.

Enantioselectivity determining transition state

From the overall Gibbs energy profile (Figure 3, main text), we see that the enantioselectivity-determining step is the initial phosphoric acid catalyzed addition of water to the bridged biaryl substrate. For each of the enantiomers, (*R*)-**1a** and (*S*)-**1a**, the water molecule can add either to the Re or the Si face of the imine group, giving rise to a total of 4 distinct transition states (TSs). Due to the bulky side groups on the chiral phosphoric acid catalyst, conformational rigidity is determined by the phosphoric acid moiety, which has to be oriented with the imine group in specific spatial arrangement for the catalyzed water addition. This gives rise to only limited conformational freedom in the possible TSs. Figure S8 shows the DFT-optimized TS structures, their HOMO and LUMO plots as well as non-covalent interaction (NCI) plots and their activation barriers relative to substrate **1a**. The frontier molecular orbitals (FMOs) in these TSs have quite similar structure, where the coefficients of the HOMOs are predominantly on the acid catalyst and the coefficients of the LUMOs are predominantly on the substrate. This potentially reflects similar electronic influences in these TSs. The NCI plots suggest that (*R*)-**TS-Si** may be most favorable as it has the least steric repulsions.

	(<i>R</i>)-TS1-Si	(<i>R</i>)-TS1-Re
ΔG^\ddagger	16.5 kcal mol ⁻¹	27.8 kcal mol ⁻¹
DFT structure		
HOMO		
LUMO		

NCI		
		
	(S)-TS1-Si	(S)-TS1-Re
ΔG^\ddagger	20.6 kcal mol ⁻¹	24.0 kcal mol ⁻¹
DFT structure		
HOMO		

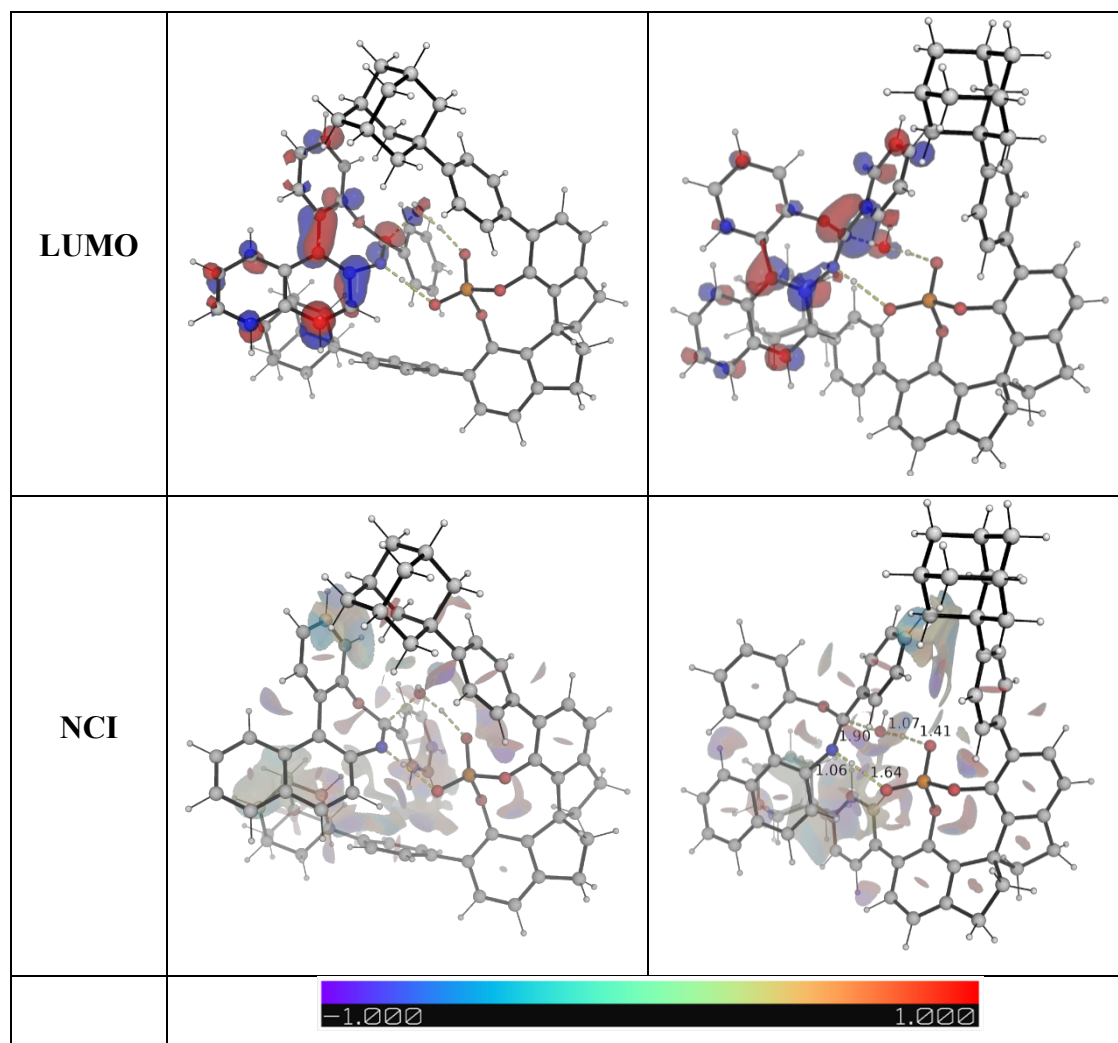


Figure S8. DFT-optimized TS structures, their HOMOs and LUMOs (isosurface value = 0.05 au) and non-covalent interaction (NCI) plots. Key bond distances are given in Å. Activation barriers (ΔG^\ddagger) are given in kcal mol⁻¹ and taken relative to the starting materials.

Transition state structures for the product formation

The DFT-optimized TS structures for the phosphoric acid catalyzed ring opening of intermediate from the addition of water (most favorable pathway) is shown in Figure S9.

	<i>(R)</i> -TS2	<i>(S)</i> -TS2
ΔG^\ddagger	8.6 kcal mol ⁻¹	9.3 kcal mol ⁻¹

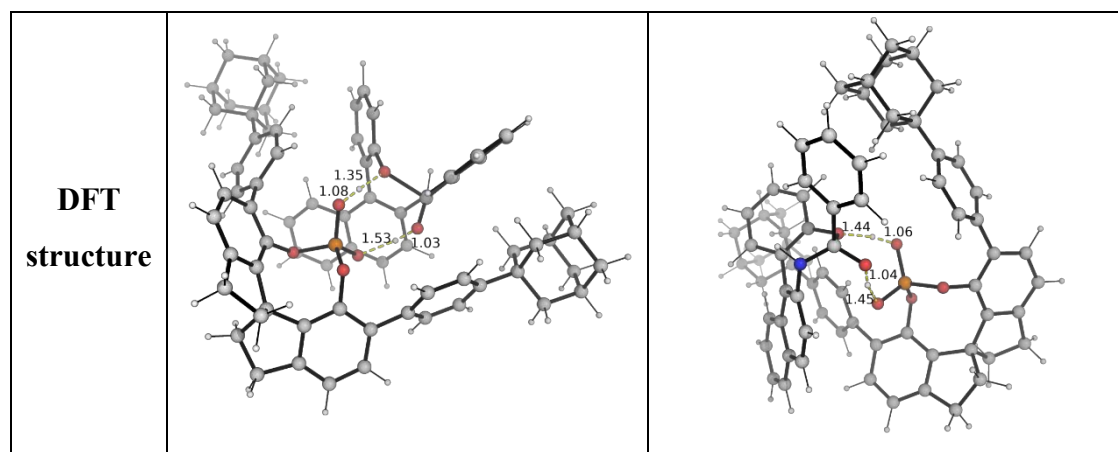


Figure S9. DFT-optimized transition state structures for the acid-catalyzed ring opening of intermediate (R)-INT3. Activation barriers are taken relative to the sum of substrates as reference zero.

Optimized structures and absolute energies, zero-point energies

Geometries of all optimized structures (in .xyz format with their associated energy in Hartrees) and movies of relevant IRC analyses are included in a separate folder named *DFT_structures* with an associated readme.txt file. All these data have been deposited with this Supporting Information and uploaded to zenodo.org (DOI: 10.5281/zenodo.7602173; <https://zenodo.org/record/7602173>).

Absolute values (in Hartrees) for SCF energy, zero-point vibrational energy (ZPE), enthalpy and quasi-harmonic Gibbs free energy for M06-2X/def2-SVP optimized structures and single point corrections in SMD(cyclohexane) using M06-2X/def2-TZVP functional are also included.

Reaction in cyclohexane at room temperature						
Structures	E/au	ZPE/au	H/au	T.S/au	qh-G/au	SP SMD(cyclohexane) M06-2X/def2-TZVP
water	-76.323214	0.021594	-76.29784	0.018411	-76.316251	-76.429369
R-C2_cat	-2537.734548	0.904737	-2536.788	0.112701	-2536.891851	-2540.331660
R-1a	-1014.316428	0.318103	-1013.98	0.061097	-1014.038693	-1015.442466

TS_rot1	-1014.288938	0.317502	-1013.9537	0.059473	-1014.011176	-1015.414776
S-1a	-1014.316428	0.318103	-1013.98	0.061097	-1014.038693	-1015.442466
R-INT1-Si	-3628.443719	1.249654	-3627.1316	0.151665	-3627.271814	-3632.238532
R-TS1-Si	-3628.432378	1.249944	-3627.1215	0.147361	-3627.258434	-3632.223761
R-INT2-Si	-3628.466462	1.253748	-3627.1515	0.149859	-3627.289614	-3632.253218
R-TS1-Re	-3628.409266	1.249009	-3627.0991	0.150678	-3627.237514	-3632.203605
S-INT1-Si	-3628.437162	1.248541	-3627.1255	0.155334	-3627.267942	-3632.237811
S-TS1-Si	-3628.421475	1.249543	-3627.1108	0.149913	-3627.248844	-3632.215960
S-INT2-Si	-3628.452169	1.253174	-3627.1376	0.151228	-3627.276462	-3632.245884
S-TS1-Re	-3628.414063	1.250004	-3627.103	0.149414	-3627.24093	-3632.211044
R-INT3	-1090.675017	0.34626	-1090.309	0.064039	-1090.370238	-1091.891815
TS_rot2	-1090.6364	0.345853	-1090.2714	0.062758	-1090.331538	-1091.853314
S-INT3	-1090.676097	0.3467	-1090.3098	0.063627	-1090.370726	-1091.893308
R-INT4	-3628.448013	1.251648	-3627.1348	0.15264	-3627.274171	-3632.240326
R-TS2	-3628.442394	1.248294	-3627.1331	0.149825	-3627.27096	-3632.233872
R-INT5	-3628.470656	1.250559	-3627.1577	0.153929	-3627.298814	-3632.263293
S-INT4	-3628.452779	1.253011	-3627.1384	0.150978	-3627.27698	-3632.244778
S-TS2	-3628.43978	1.247804	-3627.131	0.150125	-3627.268982	-3632.232122
S-INT5	-3628.469607	1.250918	-3627.1563	0.1545	-3627.297551	-3632.263464
R-2a	-1090.690151	0.345055	-1090.3241	0.068524	-1090.388493	-1091.911672

References

- [1] Liang, Y.; Ji, J.; Zhang, X.; Jiang, Q.; Luo, J.; Zhao, X. Enantioselective construction of axially chiral amino sulfide vinyl arenes by chiral sulfide-catalyzed electrophilic carbothiolation of alkynes. *Angew. Chem., Int. Ed.* **2020**, *59*, 4959-4964.
- [2] Cho, J. Y.; Roh, G.-b.; Cho, E. J. Visible-light-promoted synthesis of dibenzofuran derivatives. *J. Org. Chem.* **2018**, *83*, 805-811.
- [3] Wang, M.; Liu, Y.; Wang, L.; Lu, H.; Feng, L.; Gao, H. Cascade Chan-Lam C–O coupling/[3,3]-rearrangement of arylhydroxylamines with arylboronic acids toward noblin analogues. *Adv. Synth. Catal.* **2021**, *363*, 1733-1738.
- [4] Yang, Y.; Zhu, S.-F.; Duan, H.-F.; Zhou, C.-Y.; Wang, L.-X.; Zhou, Q.-L. Asymmetric Reductive Coupling of Dienes and Aldehydes Catalyzed by Nickel Complexes of Spiro Phosphoramidites: Highly Enantioselective Synthesis of Chiral Bishomoallylic Alcohols. *J. Am. Chem. Soc.* **2007**, *129*, 2248-2249.
- [5] a) Ahmed, A.; Bragg, R. A.; Clayden, J.; Lai, L. W.; McCarthy, C.; Pink, J. H.; Westlund, N.; Yasin, S. A., Barriers to rotation about the chiral axis of tertiary aromatic amides. *Tetrahedron* **1998**, *54*, 13277-13294; b) Curran, D. P.; Liu, W.; Chen, C. H.-T., Transfer of Chirality in Radical Cyclizations. Cyclization of o-Haloacrylanilides to Oxindoles with Transfer of Axial Chirality to a Newly Formed Stereocenter. *J. Am. Chem. Soc.* **1999**, *121*, 11012-11013.

Full reference for Gaussian software:

Gaussian 16, Revision B.01, Frisch, M. J.; Trucks, G. W.; Schlegel, H. B.; Scuseria, G. E.; Robb, M. A.; Cheeseman, J. R.; Scalmani, G.; Barone, V.; Mennucci, B.; Petersson, G. A.; Nakatsuji, H.; Caricato, M.; Li, X.; Hratchian, H. P.; Izmaylov, A. F.; Bloino, J.; Zheng, G.; Sonnenberg, J. L.; Hada, M.; Ehara, M.; Toyota, K.; Fukuda, R.; Hasegawa, J.; Ishida, M.; Nakajima, T.; Honda, Y.; Kitao, O.; Nakai, H.; Vreven, T.; Montgomery Jr., J. A.; Peralta, J. E.; Ogliaro, F.; Bearpark, M.; Heyd, J. J.; Brothers, E.; Kudin, K. N.; Staroverov, V. N.; Kobayashi, R.; Normand, J.; Raghavachari, K.; Rendell, A.; Burant, J. C.; Iyengar, S. S.; Tomasi, J.; Cossi, M.; Rega, N.; Millam, J. M.; Klene, M.; Knox, J. E.; Cross, J. B.; Bakken, V.; Adamo, C.; Jaramillo, J.; Gomperts, R.; Stratmann, R. E.; Yazyev, O.; Austin, A. J.; Cammi, R.; Pomelli, C.; Ochterski, J. W.; Martin, R. L.; Morokuma, K.; Zakrzewski, V. G.; Voth, G. A.; Salvador, P.; Dannenberg, J. J.; Dapprich, S.; Daniels, A. D.; Farkas, Ö.; Foresman, J. B.; Ortiz, J. V.; Cioslowski, J.; Fox, D. J. Gaussian, Inc., Wallingford CT, 2016.

- [6] Bannwarth, C.; Ehlert, S.; Grimme, S. GFN2-XTB - An Accurate and Broadly Parametrized Self-Consistent Tight-Binding Quantum Chemical Method with

- Multipole Electrostatics and Density-Dependent Dispersion Contributions. *J. Chem. Theory Comput.* **2019**, *15* (3), 1652–1671.
- [7] Grimme, S.; Bannwarth, C.; Shushkov, P. A Robust and Accurate Tight-Binding Quantum Chemical Method for Structures, Vibrational Frequencies, and Noncovalent Interactions of Large Molecular Systems Parametrized for All Spd-Block Elements ($Z = 1-86$). *J. Chem. Theory Comput.* **2017**, *13* (5), 1989–2009.
- [8] Bannwarth, C.; Caldeweyher, E.; Ehlert, S.; Hansen, A.; Pracht, P.; Seibert, J.; Spicher, S.; Grimme, S. Extended Tight-Binding Quantum Chemistry Methods. *Wiley Interdiscip. Rev. Comput. Mol. Sci.* **2021**, *11* (2).
- [9] Grimme, S. Exploration of Chemical Compound, Conformer, and Reaction Space with Meta-Dynamics Simulations Based on Tight-Binding Quantum Chemical Calculations. *J. Chem. Theory Comput.* **2019**, *15* (5), 2847–2862.
- [10] Pracht, P.; Bohle, F.; Grimme, S. Automated Exploration of the Low-Energy Chemical Space with Fast Quantum Chemical Methods. *Phys. Chem. Chem. Phys.* **2020**, *22* (14), 7169–7192.
- [11] Frisch, M. J. .; Trucks, G. W. .; Schlegel, H. B. .; Scuseria, G. E. .; Robb, M. A. .; Cheeseman, J. R. .; Scalmani, G. .; Barone, V. .; Petersson, G. A. .; Nakatsuji, H. .; et al. Gaussian 16, Revision B.01. 2016.
- [12] Zhao, Y.; Truhlar, D. G. The M06 Suite of Density Functionals for Main Group Thermochemistry, Thermochemical Kinetics, Noncovalent Interactions, Excited States, and Transition Elements: Two New Functionals and Systematic Testing of Four M06-Class Functionals and 12 Other Function. *Theor. Chem. Acc.* **2008**, *120* (1), 215–241.
- [13] Weigend, F.; Ahlrichs, R. Balanced Basis Sets of Split Valence, Triple Zeta Valence and Quadruple Zeta Valence Quality for H to Rn: Design and Assessment of Accuracy. *Phys. Chem. Chem. Phys.* **2005**, *7* (18), 3297–3305.
- [14] Weigend, F. Accurate Coulomb-Fitting Basis Sets for H to Rn. *Phys. Chem. Chem. Phys.* **2006**, *8* (9), 1057–1065.
- [15] Marenich, A. V.; Cramer, C. J.; Truhlar, D. G. Universal Solvation Model

- Based on Solute Electron Density and on a Continuum Model of the Solvent Defined by the Bulk Dielectric Constant and Atomic Surface Tensions. *J. Phys. Chem. B* **2009**, *113* (18), 6378–6396.
- [16] Luchini, G.; Alegre-Requena, J. V.; Funes-Ardoiz, I.; Paton, R. S.; Pollice, R. GoodVibes: Automated Thermochemistry for Heterogeneous Computational Chemistry Data. **2020**, *9*, 291.
- [17] Contreras-García, J.; Johnson, E. R.; Keinan, S.; Chaudret, R.; Piquemal, J. P.; Beratan, D. N.; Yang, W. NCIPLLOT: A Program for Plotting Noncovalent Interaction Regions. *J. Chem. Theory Comput.* **2011**, *7* (3), 625–632.
- [18] Schrödinger, L. *The PyMOL Molecular Graphics Development Component, Version 1.8*; 2015.
- [19] Fukui, K. The Path of Chemical Reactions - The IRC Approach. *Acc. Chem. Res.* **1981**, *14* (12), 363–368.
- [20] Fukui, K. Formulation of the Reaction Coordinate. *J. Phys. Chem.* **2005**, *74* (23), 4161–4163.
- [21] Yang, X.; Wei, L.; Wu, Y.; Zhou, L.; Zhang, X.; Chi, Y. R. Atroposelective Access to 1,3-Oxazepine-Containing Bridged Biaryls via Carbene-Catalyzed Desymmetrization of Imines. *Angew. Chem. Int. Ed.* **2022**, *62* (1), e202211977.